Ionic transport properties of lithium polysulfides within poly(ethylene-oxide) homopolymer electrolytes

Ernest Ahiavi, Priscillia Soudant, Didier Devaux, Renaud Bouchet

Ionic transport properties of lithium polysulfides within poly(ethylene-oxide) homopolymer electrolytes

Ernest Ahiavi[(a)], Priscillia Soudant[(a)], Didier Devaux [(a)**], Renaud Bouchet[(a)**]

(a) Univ. Grenoble Alpes, Univ. Savoie Mont Blanc, CNRS, Grenoble INP*, LEPMI, 38000 Grenoble, France

*Institute of Engineering and Management Univ. Grenoble Alpes

**Corresponding authors: renaud.bouchet@grenoble-inp.fr & didier.devaux@cnrs.fr

Abstract

Lithium-sulfur (Li-S) batteries are attractive due to their high theoretical specific energy density, nonetheless, their upscaling and widespread adaptation have been hampered by issues such as the dissolution and shuttling of lithium polysulfides species (Li_2S_x, $2 \leq x \leq 8$) from the positive electrode through the electrolyte to the negative electrode. The electrolyte medium is thus a decisive factor in tackling the lithium polysulfide shuttle mechanism. In this study, the thermodynamical, structural, and ionic transport properties of Li_2S_x within poly(ethylene-oxide), PEO, a solid-polymer electrolyte that can potentially be used in all-solid-state Li-S batteries have been investigated. Results from thermodynamical, infrared spectroscopy and XRD characterizations show that Li_2S_8 solubilizes better in PEO homopolymer compared to Li_2S_4 salt. In terms of ionic transport properties, the diffusion measurements via electrochemical methodologies also demonstrate that PEO can slow down the shuttling speed of S_8^{2-} and S_4^{2-} by almost an order of magnitude compared to a conventional liquid electrolyte such as DOL/DME. Long-chain polysulfides in PEO homopolymer show more pronounced shuttling than the short-chain polysulfide. These findings may guide the design of adapted solid polymer electrolytes that can be used as binders or electrolyte separators for all-solid-state Li-S batteries.

Keywords

Solid polymer electrolyte; lithium polysulfides; thermodynamical properties; transference number, diffusion coefficient.

Introduction

The need for batteries in portable electronic devices, stationary storage, and electric mobilities, makes them ubiquitous [1]. Despite Li-ion battery's market domination, there is a growing demand for safer [2], better performing [3], affordable, and environmentally friendly batteries which calls for the need to pursue other battery chemistries. Among those, lithium-sulfur (Li-S) batteries can theoretically deliver energy densities ten times higher than what the current Li-ion battery offers [4]. Besides its ability to store high amounts of energy, sulfur is cost-effective, abundant, nontoxic, and environmentally friendly [5]. Lithium is also the lightest of all metals, having the lowest standard potential (-3.05 V *vs*. Li/Li^+) [6], and possesses a very high theoretical specific capacity (3860 $mAh.g^{-1}$) [7]. Marrying these properties give Li-S batteries a large storage capability of 2500 $Wh.kg^{-1}$ in theoretical energy density based on the two-electron transfer per S atom [8].

Despite intense development in the past decade, the scale-up and widespread adaptation of this promising technology is impeded by tremendous challenges; prominent among them is the dissolution and transport of intermediate products (lithium polysulfides, Li_2S_x, $2 \leq x \leq 8$) within the electrolyte in a redox shuttle process which reduces the faradic efficiency and affects the cycle life [4]. Li_2S_x reacts with the Li negative electrode forming an insulating layer thereby increasing the internal resistance of the cell and eventual capacity fading [5]. One crucial point is that the dynamics of polysulfide driving the rate of shuttling depend on the nature of the electrolyte, usually a mixture of 1, 3-dioxolene (DOL) and 1,2-dimethoxyethane (DME) with a Li salt and its additives (e.g., $LiNO_3$) when a liquid electrolyte is used [4].

To improve the performance of the Li-S battery, several strategies have been devised in an attempt to confine Li_2S_x within the positive electrode volume using architectured active materials [9–12], functionalized separators [13–15] or protective layer on the Li surface [16–18]. Some of these approaches may be efficient but are often too complex to be cost-effective in industrial applications. Moreover, the use of high-capacity sulfur-positive active material leads to high current densities even at low battery cycling rates facilitating the onset of dendrite growth on the Li metal electrode. Therefore, to tackle the issues of polysulfide shuttle and dendrite growth, replacing the liquid electrolyte with a dendrite-resistant solid-based electrolyte is of interest as its functionalities can be tailored.

Among the families of solid electrolytes, solid polymer electrolytes (SPEs) based on poly(ethylene oxide) (PEO) are promising thanks to their ionic conductivity (σ), high enough at temperatures (T) above the PEO melt (T_m, typically at 55 – 60 °C), relatively high Gutmann donor number [19] and their electrochemical stability window compatible with sulfur [20]. In an important piece of work, the group of N. P. Balsara reported on the effect of Li_2S_x ($2 \leq x \leq 8$) chain length on the thermodynamical and electrochemical properties with a specific focus on PEO homopolymers and diblock copolymer electrolytes [21, 22]. The interest of such a study is to mimic Li-S battery failure when Li_2S_x diffuses within the PEO-based electrolyte. To achieve a functional battery system, Armand, and Rodriguez-Martinez et *al*. investigated the dissolution of polysulfides in polyethylene

oxide (PEO) [23–25]. Their studies also focused on optimizing the cell assembly and its chemistry, particularly using additives. Notably, they successfully documented the cycling behavior of Li metal batteries.

To go further, a comprehensive study of the effect of chain length, and concentration of lithium polysulfides on the ambipolar diffusion coefficient (D_{amb}) and cationic transference number (T^+) would help to fully understand Li polysulfide transport in the PEO homopolymer. Indeed, since lithium polysulfides are ionic, they can be considered as Li salt and their solvation, degree of dissociation and transport in SPEs can be described by the three ionic transport properties (σ, T^+, and D_{amb}).

Herein, solid polymer electrolytes were formulated in a controlled inert atmosphere to avoid any moisture contamination by filling high molecular weight PEO homopolymer with lithium polysulfides (Li_2S_x, x = 4, 8) at different concentrations. The goal is to assess the PEO efficiency to solubilize lithium polysulfide and to understand the resulting ionic transport properties within the PEO matrix. For this, thermodynamical properties are reported using differential scanning calorimetry (DSC) while X-ray diffraction (XRD) sheds light on the PEO crystal structuration and the vibration modes of bonds are analyzed using Fourier transform infrared spectroscopy (FTIR) and finally, the three ionic transport properties (σ, T^+, and D_{amb}) are investigated by the means of electrochemical methodologies. The results show a strong impact of polysulfides on the transference number compared to PEO mixed with a conventional Li salt (LiTFSI), while the Li^+ diffusion coefficient seems to be independent of the concentration of the lithium polysulfides or the nature of the anion. In addition, FTIR is shown to be an efficient tool to study polysulfide solubility in the PEO matrix.

1 Experimental

1.1 Materials

High molecular weight (M_n, 100 kg.mol^{-1}) poly(ethylene oxide), (PEO, Alfa Aesar) homopolymer and lithium bis(trifluoromethanesulfonyl)imide (LiTFSI, Merck) were dried under vacuum for several days at 90 °C and 120 °C respectively and placed in an argon (Ar) glovebox (H_2O and O_2 < 1 ppm). In addition, powders of lithium sulfide (Li_2S, Thermo Scientific, 99.9 %) and sulfur (S_8, Alfa Aesar, 99.5 %) were also dried in a vacuum chamber (desiccator, Vacuo-Temp) placed directly inside the Ar glove box.

1.2 SPE formulation

As reference solid polymer electrolyte (SPE), PEO/LiTFSI films were formulated by dissolving different mole ratios (EO/Li) of PEO and LiTFSI in acetonitrile (Merck, 99.8 %). The mixtures

were stirred magnetically overnight at 60 °C in an Ar glovebox (H_2O and O_2 < 1 ppm) until a homogeneous solution was obtained before casting into a polytetrafluoroethylene Petri dish. The solvent was evaporated at room temperature in the glovebox and finally, the Petri dish containing the semi-dried membrane was placed in a desiccator to be vacuum-dried at 60 °C overnight. A schematic of the SPE formulation process is shown in **Figure S1**. The resulting dry SPEs were peeled off the Petri dish and then transferred into a solvent-free Ar glovebox dedicated to electrochemical cell assembly for at least two weeks before any characterization. Similarly, PEO was formulated with different concentrations of lithium polysulfides. For these, the polymer was first dissolved in acetonitrile at 60 °C and mixed with defined amounts of a prepared solution of Li_2S_x (x = 4 or 8) in the same solvent before casting. For the latter solution, Li_2S and S_8 were mixed in stoichiometric amounts in acetonitrile and stirred overnight to obtain a uniform solution. The reaction equation to obtain a known quantity of Li_2S_x is [21, 22]:

$$Li_2S + \frac{(x-1)}{8}S_8 \rightarrow Li_2S_x \qquad (x = 4 \text{ or } 8) \tag{1}$$

The lithium polysulfide concentration in the polymer is presented as the molar ratio R, varied between 0 and 0.12 based on the work of Wang et *al.* [21, 22]:

$$R = \frac{n(Li_2S_x)}{n(polymer)} \tag{2}$$

1.3 Differential scanning calorimetry (DSC)

The thermodynamical properties of the SPEs with varying salt concentrations (R) were determined using differential scanning calorimetry (DSC 1, Mettler Toledo). The SPE samples were sealed in hermetic Aluminium pans in the glovebox before measurements. All samples were heated up to 130 °C (at 5 °C/min), cooled down to -100 °C (at 10 °C/min) and heated again to 120 °C (at 5 °C/min). The glass transition temperature (T_g), melting temperature (T_m) and the enthalpy of melting ΔH_m were all extracted from the second heating scan. As a typical example, the thermogram of PEO/Li_2S_8 at R = 0.008 is shown in **Figure S2** indicating that the T_g values were extracted from the mid-point of the glass transition and T_m from the intersection of the tangent and the baseline of the heat flow transition (onset of the T_m). Then, the degree of crystallinity (X_c) was calculated according to **eq. 3**.

$$X_c = \frac{\Delta H_m}{\Delta H_m^o} * 100\ \% \tag{3}$$

With ΔH_m the enthalpy of melting of the SPE and ΔH_m^o is the enthalpy of melting of a 100 % crystalline PEO taken as 195 $J.g^{-1}$ [26].

1.4 Density of PEO/Li_2S_x

The density of the PEO/Li_2S_x electrolyte was measured based on Archimedes principles by using a standard density kit (Mettler Toledo) placed on a balance inside an Ar-filled glovebox. At room temperature, the weight of a PEO/Li_2S_x dry mixture was measured in Argon (density, ρ_{Ar} = 0.0016 g.cm^3) and heptane ($\rho_{heptane}$ = 0.6692 g.cm^3). The density of the SPE (ρ_{PEO/Li_2S_x}) was calculated according to **eq. 4**.

$$\rho_{PEO/Li_2S_x} = \frac{weight\ in\ Ar}{weight\ in\ Ar - weight\ in\ heptane} * \left(\rho_{heptane} - \rho_{Ar}\right) + \rho_{Ar} \quad (4)$$

For comparison purposes, the theoretical density of the PEO/Li_2S_x electrolyte assuming an ideal mixture was calculated according to:

$$\rho_{PEO/Li_2S_x} = \frac{M_{EO/Li_2S_x}}{V_{EO/Li_2S_x}} = \frac{\left(M_{EO} + R * M_{Li_2S_x}\right)}{\left(V_{EO} + R * V_{Li_2S_x}\right)} \quad (5)$$

The molar mass of PEO/Li_2S_x was calculated using a linear combination of the individual molar masses:

$$M_{EO/Li_2S_x} = \left(n_{EO} * M_{EO}\right) + \left(n_{Li_2S_x} * M_{Li_2S_x}\right) \quad (6)$$

The volume of the mixture was calculated by considering the ratio of masses and molar masses (*m/M*) for each compound where the partial molar volume of PEO was taken to be 38.5 cm^3.mol^{-1} [27]:

$$V_{EO/Li_2S_x} = \left(n_{EO} * V_{EO}\right) + \left(n_{Li_2S_x} * V_{Li_2S_x}\right) \quad (7)$$

Likewise, the molar mass and volume of the Li_2S_x assuming an ideal mixture, were calculated using **eq. 8** and **eq. 9** respectively.

$$M_{Li_2S_x} = \left(\frac{1-x}{8}\right) * M_{S_8} + M_{Li_2S} \quad (8)$$

$$V_{Li_2S_x} = \left(\frac{1-x}{8}\right) * V_{S_8} + V_{Li_2S} \quad (9)$$

Here the partial molar volumes of S_8 and Li_2S were taken to be 123.9 cm^3.mol^{-1} and 27.7 cm^3.mol^{-1} respectively [28, 29]. The molar mass of S_8 (M_{S8}) and Li_2S (M_{Li2S}) were taken to be 256.52 g.mol^{-1} and 44.95 g.mol^{-1} respectively.

1.5 Fourier transformed Infrared spectroscopy (FTIR)

SPE solutions of polymer/salt dissolved in acetonitrile were coated onto a ZnSe window (PerkinElmer) inside the Ar-filled glovebox. Subsequently, the solvent was evaporated by placing

the sample in a desiccator under vacuum in a similar fashion as used for the SPE formulation. This process resulted in the formation of thin SPE films of about ≤ 1.5 μm thick. To ensure airtightness when the samples were taken outside the glovebox for measurement, a parafilm mask was placed on the facing edges of the ZnSe window and firmly pressed together. The FTIR spectra were recorded using PerkinElmer Spectrum 2 FTIR spectrometer in transmission mode, within 800 - 1500 cm^{-1} range with 1 cm^{-1} resolution.

1.6 X-ray diffraction (XRD)

X-ray diffraction was carried out using a diffractometer X'Pert Pro (Malvern PANAnalytical) equipped with a Bragg-Brentano geometry at the Consortium des Moyens Technologiques Communs (CMTC Grenoble INP, France) platform. A Cu-Kα anode (λ = 1.5406 Å) was used with a 2θ angle ranging from 6 ° to 60 ° with 0.05 ° intervals. Inside the Ar-filled glovebox, SPEs were filled into capillaries made of borosilicate glass and sealed using a resin to avoid exposure to air. Phase identification was performed using DIFFRAC.EVA (Bruker) phase indexing software by comparing the diffractograms to a reference database.

1.7 Scanning electron microscopy and energy dispersive X-ray spectroscopy

Scanning electron microscopy (SEM) and energy dispersive X-ray spectroscopy (EDX) were used to study the particle size and composition of the sulfur powder (S_8) respectively. The measurements were performed at the CMTC platform using a scanning electron microscope (Ultra 55 SEM FEG, Zeiss, Jena, Germany) operated at 5 kV.

1.8 Ionic conductivity

The ionic conductivity (σ) of the SPEs was determined using Li symmetric coin cells (CR2032) by sandwiching the SPE of known thickness (l) within a polypropylene spacer (to maintain a fixed active surface area, A of 10 mm diameter) between two Li foils stacked to stainless steel current collectors. For completeness, impedance was also measured using stainless steel blocking electrodes and compared to non-blocking ones.[30] The results for PEO/Li_2S_4 are displayed in **Figure S3** showing a full agreement of the bulk contribution and resulting ionic conductivities for the two types of symmetric cells. In the glove box, the Li/SPE/Li cells were first assembled using a homemade laminating machine held at 80 °C and 3 bars to ensure intimate contact between the layers, before being sealed in the coin cell. The cells were then placed in an oven (Clima Temperature System) and connected to a potentiostat with impedance capability (VMP300, BioLogic). Electrochemical impedance spectroscopy was performed at a given temperature (T) using an excitation signal of 40 mV in the frequency range between 7 MHz and 100 mHz. The temperature program consisted of heat-cool-heat scans from 25 °C to 100 °C by step of 5 °C. Each impedance spectrum was fitted using Z-View software (Scribner Inc.) to extract the bulk electrolyte

(R_{bulk}) and the interface resistances (R_{int}). The electrical equivalent circuit is the sum of the cable and instrument resistances and inductance at high frequencies, followed by the electrolyte response fitted with a resistance in parallel with a pseudo-capacitance for $T > T_m$ and just a resistance for $T > T_m$, followed by another resistance in parallel with a pseudo-capacitance for the Li/SPE interfaces. As an example, the impedance spectrum and its best fit ($\chi^2 > 0.99$) of a Li symmetric cell comprising the PEO/Li_2S_4 (R = 0.03) recorded at 90 °C is displayed in **Figure S4**. Then σ was calculated using the usual relationship:

$$\sigma = \frac{l}{A * R_{bulk}} \tag{10}$$

1.9 Transference number

The cationic transference number (T^+) was calculated using the Bruce and Vincent method [31] by applying the Watanabe equation [32]. Typically, a Li symmetrical cell is potentiostatically polarized by a constant potential (ΔV *vs*. Li^+/Li) at 80 °C and the current (I) response is recorded over time until a steady state (I_s) is reached. An example of such a polarization is provided in **Figure S5a** for the PEO/Li_2S_4 (R = 0.03) at 80 °C. The bulk and interface resistances are determined before and after polarization by fitting the impedance spectra exemplified in **Figure S5b** for the same electrolyte. T^+ was calculated using the following equation [32]:

$$T^+ = \frac{R_{bulk}}{\left({}^{\Delta V}/_{I_s} - R_{int}\right)} \tag{11}$$

1.10 Ambipolar diffusion coefficient

The ambipolar diffusion coefficient (D_{amb}) was determined based on the restricted diffusion technique from Newman and Chapman [33] by allowing the previously polarized Li symmetrical cell to relax while the cell potential (ΔV *vs*. Li^+/Li) is recorded over a typical time (t) of 3 hours. **Figure S5c** represents such a relaxation profile in the logarithm scale for the PEO/Li_2S_4 (R = 0.03) electrolyte at 80 °C. The slope of the linear part of *-ln* (ΔV) *vs*. time (t) corresponds to the characteristic diffusion time (τ_d) of the ionic species. Then, D_{amb} was calculated according to **eq. 12** [34].

$$D_{amb} = \frac{\tau_d * l^2}{\pi^2} \tag{12}$$

By definition, the ambipolar diffusion coefficient can be written as a function of the cationic (D^+) and anionic (D^-) diffusion coefficients as:

$$D_{amb} = \frac{2D^+D^-}{D^+ + D^-} \quad (13)$$

$$D^+ = \frac{D_{amb}}{2(1-t^+)} \quad (14)$$

$$D^- = \frac{D_{amb}}{2 * t^+} \quad (15)$$

2 Results and Discussion

2.1 Density of PEO/Li_2S_x

The density ($\rho_{PEO/Li2Sx}$) of PEO/Li_2S_x electrolytes first determined in the Ar glovebox using the conventional density kit are displayed as a function of the lithium polysulfide concentration (*R)* in **Figures 1a** and **1b** for PEO/Li_2S_4 and PEO/Li_2S_8 respectively. In **Figure 1a**, the ρ of PEO/Li_2S_4 is a gradually increasing function of *R*. As a comparison, the theoretically calculated density based on **eq. 5** assuming an ideal mixture is added in **Figure 1a** as a red line. There is good agreement between the theoretical and the experimental data. In **Figure 1b**, the experimental density, $\rho_{PEO/Li2S8}$ also follows the evolution of the theoretical density with the polysulfide concentration. However, the density of PEO/Li_2S_8 has a stronger increase with *R* compared to the PEO/Li_2S_4 electrolyte. Indeed, the slope of $\rho_{PEO/Li2S8}$ is about twice that of $\rho_{PEO/Li2S4}$. Park et. *al* reported a similar difference in the slope between Li_2S_4 and Li_2S_6 in DOL/DME liquid-based electrolytes using molecular dynamic (MD) simulations [35]. Depending on the amount of S_8 or Li_2S present in the Li_2S_x, the molar volume and thus the density of the PEO/Li_2S_x change accordingly. The difference between the experimental and theoretical density results from the specific interaction between the solute and the PEO matrix. Herein, the difference is in the error margin. For Li_2S_4, the break in slope in the experimental data around $R = 0.05$ could suggest reaching the limit of solubility. The assumption of an ideal mixture for the calculation of the density of PEO/Li_2S_x is a simplification, and it becomes particularly challenging because the disproportionation reaction results in a polydisperse distribution of species rather than a single Li_2S_x species. However, on average, the lithium polysulfide mixture seems to behave as the as-prepared equivalent Li_2S_x [36].

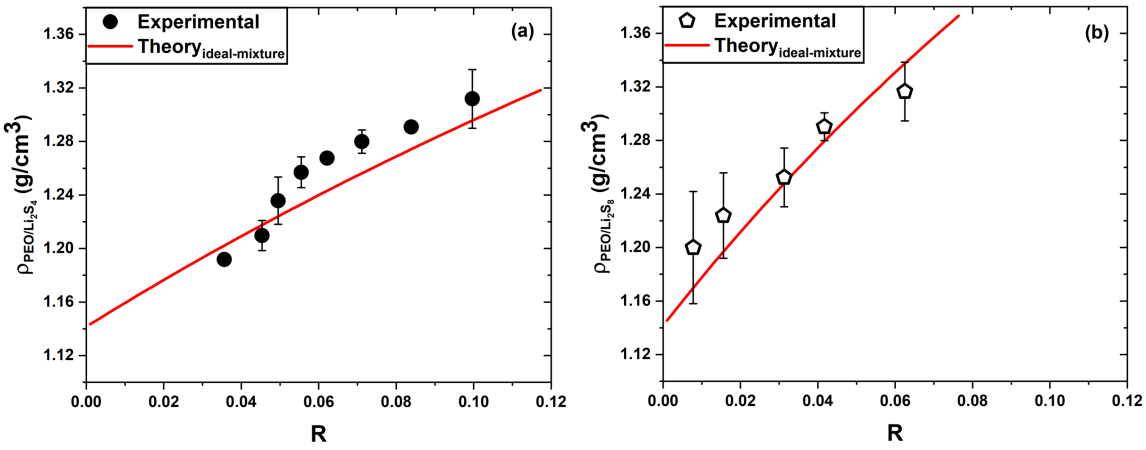

Figure 1. Experimental densities of (a) PEO/Li_2S_4 and (b) PEO/Li_2S_8. Theoretically calculated densities of the PEO/Li_2S_x are shown as a straight line (**eq. 5**) within the respective Li_2S_x.

2.2 Thermodynamical properties

DSC is a pivotal tool for understanding thermodynamical properties such as glass transition and crystallinity, which have a direct correlation to the ionic conductivity properties of polymer/salt complexes [37]. In **Figure 2**, the DSC thermograms of PEO/Li_2S_8 at different salt concentrations are shown, highlighting the glass transition temperature (T_g, **Figure 2a**) and the melting temperature (T_m, **Figure 2b**) of the PEO. In **Figure 2a**, compared to the neat PEO ($R = 0$), the T_g shifted to higher temperatures with increasing Li_2S_8 concentration. Such dependency is typical of the physical crosslinking effect of salt solvation resulting in a stiffening of the polymer chains and thus decreasing the segmental motion [38]. Also, the increasing height of the transition step with concentration suggests an increase in the amorphous content of PEO-Li_2S_8 complexes in the film. In addition, a single T_g is observed for the exemplified SPE in **Figure 2a** as well as for all the other investigated electrolytes irrespective of the nature of the lithium polysulfide and the concentration which indicates uniform composition [22]. In **Figure 2b**, T_m decreases to lower temperatures with the increase in Li_2S_8 concentration until complete amorphization which correlates to a lowering of the degree of crystallinity as the enthalpy of melting (ΔH_m) is also reduced. For all R values, the elemental sulfur (S_8) melting peak expected at about 118 °C is absent which confirms that there are no S_8 leftovers in the SPE mixtures resulting from the electrolyte formulation process [39].

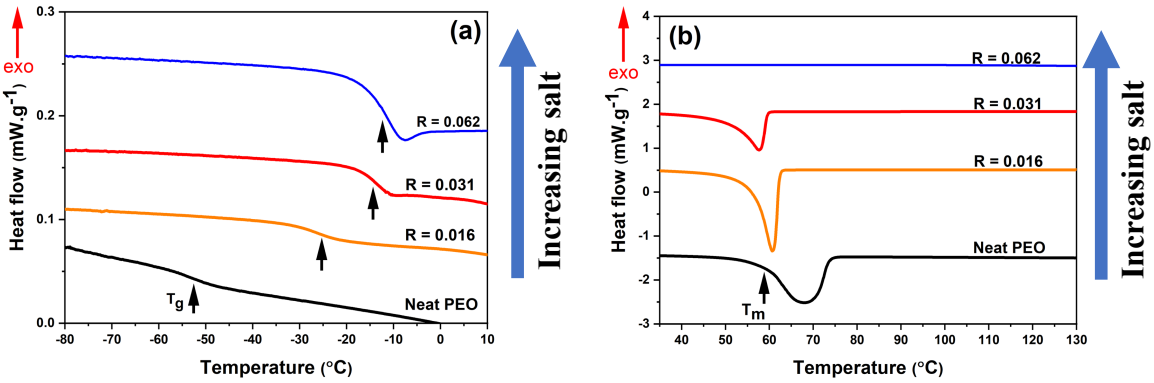

Figure 2. DSC thermograms of PEO/Li_2S_8 for different salt concentrations (R) focusing on the a) T_g and b) T_m regions. To enhance the clarity, the plots are vertically shifted.

The plot of T_g as a function of salt concentration (R) for the SPEs is shown in **Figure 3a**. As expected, the evolution of T_g with the concentration of LiTFSI (R) in PEO homopolymer is a constant increase and consistent with previous literature report [40]. The T_g of PEO/Li_2S_4 versus R is also shown in **Figure 3a**. From this plot, it can be observed that at any given R value, the T_g of PEO/Li_2S_4 is higher than that of PEO/LiTFSI. This implies that when filled with Li_2S_4 salt, the chains of the PEO homopolymer become less mobile as compared to LiTFSI. Meanwhile, the T_g of PEO/Li_2S_4 presents a pseudo-linear increase from $R = 0$ (T_g of -56 °C) until $R \sim 0.056$. After this R value, there is a drop of about 10 °C of the T_g which was verified for several replicas of the PEO doped with Li_2S_4. This drop in T_g is an indication of reaching the limit of solubility of Li_2S_4 into the PEO homopolymer. Meanwhile, the results agree well with those reported by Wang *et al.* on comparable PEO/Li_2S_4 mixtures [22]. We noted that during the drying process in the desiccator of the highest concentrated electrolytes, some elemental sulfur particles tend to cover the glass dome of the apparatus. The collected particles were analysed by SEM and EDX and the results are shown in **Figures S6a** and **b** confirm the presence of bare sulfur. This indicates that the effective salt concentration of equivalent Li_2S_4 in the polymer for $R > 0.056$ is most probably lower than the reported value and confirms the principle of limit of solubility. On the other hand, the T_g of PEO/Li_2S_8 (**Figure 3a**) also increases continuously from -54 ± 2 °C at $R = 0$ to reach a plateau at $R = 0.063$ (-13 ± 2 °C). For $R \geq 0.013$, the T_g of PEO/Li_2S_8 is slightly lower than that of the PEO/Li_2S_4 counterpart. This translates into a faster dynamic of the PEO chains for Li_2S_8 than Li_2S_4. Also, within the investigated concentration range, there was no limit to the solubility of Li_2S_8 in PEO compared to Li_2S_4. This implies that the long-chain lithium polysulfide (Li_2S_8) is more soluble in PEO homopolymer than the short-chain lithium polysulfide (Li_2S_4). So, within a Li-S battery comprising PEO electrolyte, the thermodynamic and thus the correlated ionic transport properties will evolve during cycling, depending on the state of charge as a function of the polysulfide nature (redox shuttle).

The plot of melting temperature (T_m) versus R for PEO homopolymer doped with different salts is displayed in **Figure 3b**. The T_m of PEO/LiTFSI strongly decreases with increasing R as expected [40]. The T_m of PEO/Li_2S_4 decreases strongly from the neat PEO until $R \approx 0.013$. Above this R value, the decrease in T_m is similar to PEO/LiTFSI but with higher magnitudes. Comparatively, the T_m of PEO/Li_2S_8 also shown in **Figure 3b,** decreases sharply with R until complete amorphization at $R >$ 0.06. In general, the abrupt decrease of the T_ms with increasing Li_2S_8 concentration is similar to the seminal work by Balsara's group [21, 22].

In **Figure 3c**, the plot of the degree of crystallinity (X_c) of the SPEs as a function of the concentration of the lithium salts (R) is displayed. For PEO/LiTFSI, X_c decreases with R due to the reduction in the enthalpy of melting by the presence of the salt [41]. For PEO/Li_2S_4, X_c decreases linearly with R from 74 % (neat) down to 0 % (amorphous) at R = 0.093. When the PEO homopolymer is doped with Li_2S_8, as also shown in **Figure 3c**, the decrease of X_c with R is more significant, reaching zero at $R = 0.06$. Below $R \leq 0.042$, the magnitude of X_c for PEO/Li_2S_8 is similar to that of PEO/LiTFSI electrolyte.

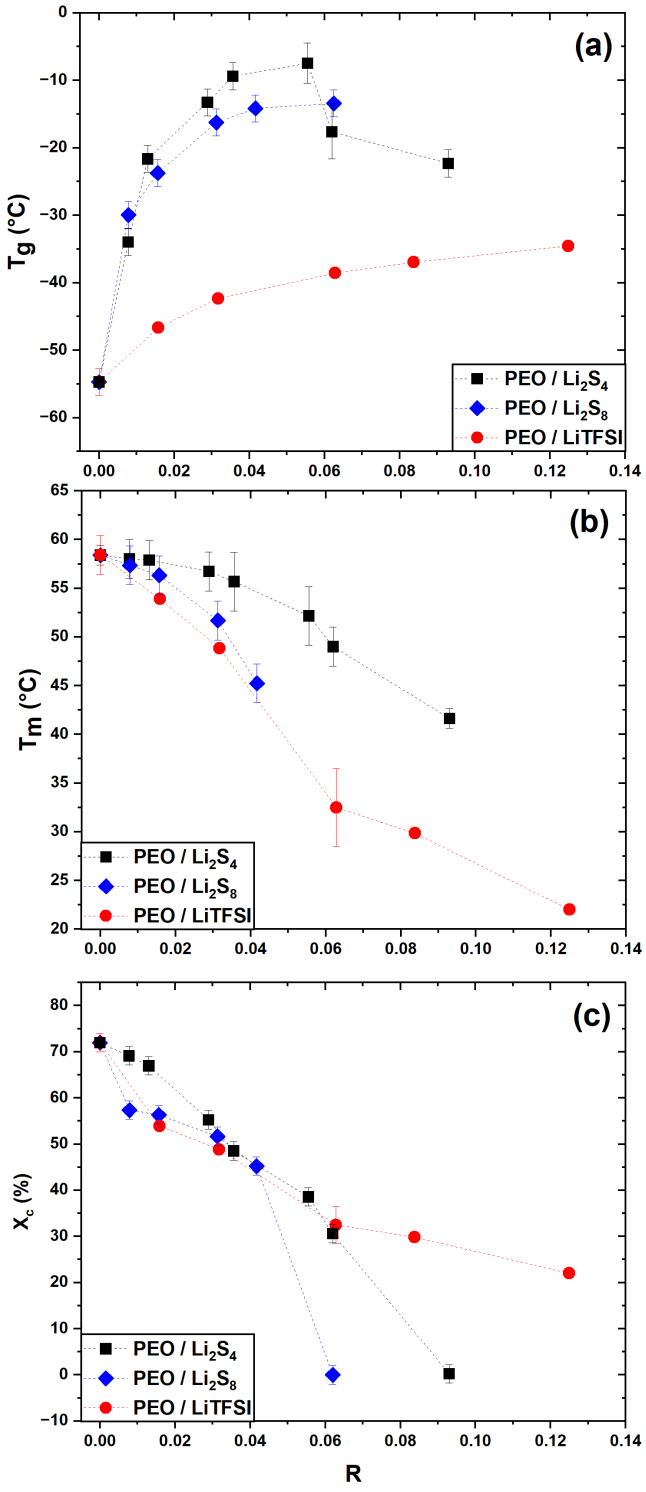

Figure 3. Thermodynamical properties of PEO doped with Li_2S_4, Li_2S_8 and LiTFSI as a function of the salt concentration (R) for the (a) glass transition temperature (T_g), (b) melting temperature (T_m) and (c) degree of crystallinity (X_c).

2.3 FTIR spectra of PEO/Li_2S_x electrolytes

The interest of performing FTIR measurements is to study the effect of the polysulfide solvation into the PEO homopolymer. But to achieve this, the effect of well-studied LiTFSI on PEO was first investigated and compared. The FTIR spectra of neat PEO bands in the 800 - 1500 cm^{-1} region, recorded at room temperature, are shown in **Figure 4a**. The vibrational peaks align well with the band positions reported in the literature [42] [43] [44, 45]. Specifically, the bands between 1061 and 1147 cm^{-1}, corresponding to the C-O-C stretching vibrations, are reported to be sensitive to complexation with Li^+ cations. In **Figure 4a**, upon the addition of LiTFSI, the relative intensity of the strong band at 1113 cm^{-1} changes with salt concentration. In the region of interest (1061 and 1147 cm^{-1}), the vibrational modes of SO_2 and CF_3 from $TFSI^-$ anion (reported in **Table 1**) overlap with the vibrations of C-O-C modes of the PEO occurring in the same frequency [43]. Due to this, it is difficult to specifically quantify the effect of the solvation of the Li^+ cations from LiTFSI by the PEO homopolymer. Therefore, the effect of Li^+ cations on the stretching mode of the C-O-C vibration is subtle. Nonetheless, it is clear from **Figure 4a** that the addition of LiTFSI salt to the PEO leads to a reduction in the crystallinity evidenced by the broadening of the peaks between the 1060 and 1148 cm^{-1}.

Assignments	Frequency (cm^{-1})
ν_a SO_2	1354, 1333
ν_s SO_2	1136
ν_a CF_3	1193
ν_s CF_3	1240
ν_a SNS	1060
C-O-C	1100, 1118, 1147

Table 1. Characteristic frequencies of SO^2 and CF_3 stretching vibrations of $TFSI^-$ from references [42] and [43], and that of the C-O-C band of the PEO. The symbols ν_s and ν_a represent symmetrical and asymmetrical stretching vibrational modes. The measurements were performed on PEO/LiTFSI (R = 0.06) at 80 °C.

The infrared absorption of the disulfide (S-S) vibrational band occurs in the 482 - 540 cm^{-1} range [46 47]. Since the region of interest lies in the range of 1000 – 1200 cm^{-1}, using thin films of PEO/Li_2S_x provides a better way compared to LiTFSI to probe the interaction between Li^+ and PEO. The molecular interactions of the PEO doped with varying concentrations of Li_2S_4, are shown in **Figure 4b**. Overall, minimal changes are observed in the peak positions of the complexes when compared to the neat PEO. This observation runs counter to the strong broadening and change of peak position, shape and intensity of the C-H bands that was reported by Fang et *al*. when a few concentrations of Li_2S_6 (≤ 5 wt %) were added to PEO [48]. However, a closer examination of the frequency at 1113 cm^{-1} (in **Figure 4b**) reveals that the peak broadens slightly as the concentration of Li_2S_4 increases. This may provide some evidence of salt solubility within the PEO. This also suggests that there is a reduction in the crystallinity of the PEO due to the crosslinking effect of Li_2S_4 as already seen in the DSC measurements.

The vibrational spectra of PEO/Li_2S_8 are shown in **Figure 4c**. At $R \leq 0.03$, there is minimal visible effect of the Li_2S_8 salt on the PEO vibrational modes except for the slight broadening of the 1113 cm^{-1} peak. However, as R increases further, the C-H and C-O-C modes of the PEO become broader and signal a stronger reduction in crystallinity. At $R = 0.06$, the distinct vibrations between 1061 and 1150 cm^{-1}, merge into a single broad peak, shifting to lower frequency. This is an indication of a strong interaction between Li_2S_8 and the PEO at this concentration leading to almost complete amorphization of the PEO. This confirms the argument that Li_2S_8 may solubilize better in PEO compared to Li_2S_4 as demonstrated by the thermodynamical analysis in **Figure 3**.

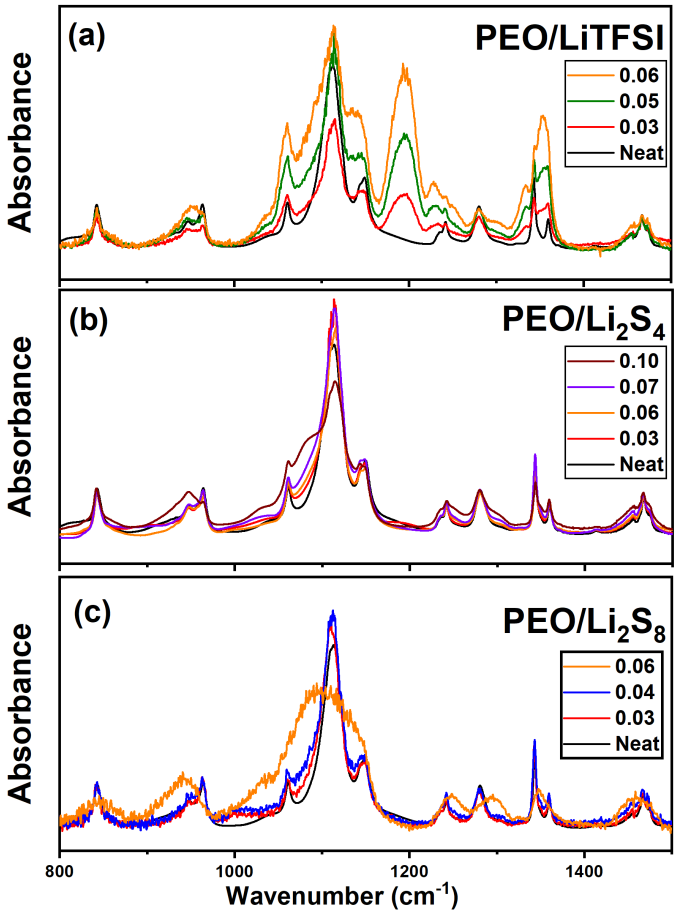

Figure 4. Infrared spectra measured at room temperature covering the region between 800 and 1500 cm^{-1} of PEO doped with (a) LiTFSI, (b) Li_2S_4 and (c) Li_2S_8 are displayed. The spectra are compared to the spectra of the neat PEO and are vertically stacked for easier comparison.

2.4 Microstructure of the PEO/Li_2S_x mixtures

To assess the impact of Li_2S_x on the microstructure of the PEO, X-ray diffraction (XRD) measurements were conducted on selected samples at room temperature. The XRD patterns of PEO/Li_2S_4 electrolytes measured at room temperature are shown in **Figure 5a**. Data obtained from neat PEO and Li_2S are given as references. The spectra for the neat PEO present the characteristic peaks of its semi-crystallinity and agree well with those reported in the literature [49, 50]. As the concentration of Li_2S_4 was increased, the intensity of the crystalline peaks especially the single *120* peak at $2\theta = 19.1°$ and the triple *032* peaks at 23.3° tend to broaden slightly while their intensities slightly decrease. There is a coalescence of the crystalline peaks at $2\theta = 13.1°$ and 13.5 into a single peak at $R = 0.09$ as can be seen clearly in the insert of **Figure 5a**. This signifies a reduction in the PEO crystallinity. However, there are two distinctive peaks (indicated by an arrow) that can be observed at $2\theta = 10.7°$ and 11.3° for $R \geq 0.02$. The presence of these peaks may be linked to a specific PEO:Li_2S_4 complex, similar to those of PEO:LiTFSI when the salt concentration reaches a certain threshold of $R > 0.042$ (*i.e.* EO/Li < 12) [51, 40]. For $R = 0.02$, apart from the peaks of the PEO and PEO:Li_2S_4 complexes, there are peaks attributed to Li_2S that are present in the diffraction

pattern whose origin could either be due to (i) trapped unreacted Li_2S from the Li_2S_4 synthesis or (ii) a disproportionation of Li_2S_4 into Li_2S and long chain polysulfides. Nevertheless, if the Li_2S originated from unreacted species, then the DSC spectra should have shown an endothermic peak at 115 °C due to the presence of a stoichiometric amount of S_8 in the polymer structure. In the absence of sulfur evaporation during SPE drying, the DSC spectra in **Figure 2b** do not display peaks attributed to sulfur melting. Therefore, spontaneous disproportionation or limited solubility of Li_2S_4 could explain the presence of Li_2S in the XRD patterns. However, a thorough investigation of this process is beyond the scope of this paper.

X-ray diffraction patterns for PEO/Li_2S_8 electrolytes are depicted in **Figure 5b**. Again, there is not much difference between the spectra of the Li_2S_8 doped samples and the neat PEO, nonetheless, there is a slight broadening of the peaks. At $R \geq 0.03$, the *110* peak has diminished in intensity and the peaks marked with asterisks (shown in the insert of **Figure 5b**) merged into a single peak. The *112* peak has become so broadened that it appears almost extinct at $R = 0.06$. These observations attest to the amorphization of the PEO/Li_2S_8 electrolytes as illustrated by both thermal and infrared measurements in **Figure 3c** and **4c** respectively.

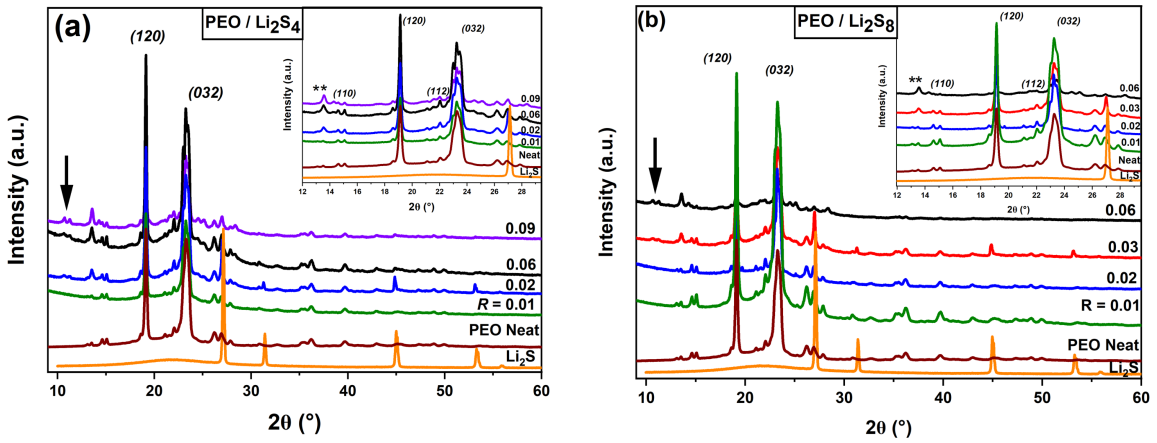

Figure 5. XRD spectra of the PEO doped with (a) Li_2S_4 salt and (b) Li_2S_8 salts. Spectra were recorded at room temperature. For clarity, the plots are vertically shifted.

2.5 Ionic transport of Li_2S_4 in PEO homopolymer

The ionic conductivities (σ) of PEO/LiTFSI and PEO/Li_2S_4 electrolytes at 80 °C are displayed as a function of salt concentration (R) in **Figure 6a**. Similarly to PEO/LiTFSI, the σ of PEO/Li_2S_4, initially increases with R due to the increase in charge carrier concentration then reaches a maximum at $R = 0.05$ before decreasing slightly [40]. The slight drop in σ has been attributed to i) an increase in the viscosity of the amorphous phase caused by the presence of a high concentration of salt and ii) the formation of ion pairs due to the increase in charge carrier concentration [52]. These effects lead to a decrease in both free ions and ionic mobility within the PEO chains. We observed that the reported ionic conductivity (σ) as well as the other ionic transport properties, transference number (T^+) and ambipolar diffusion coefficient (D_{amb}), for a 100 kg.mol^{-1} PEO/LiTFSI (see **Figure**

S8) are consistent with those reported in literature [40, 53–56,] which validates our electrolyte formulation methodology. In **Figure 6a**, the slope of the plot of log(σ) versus log(R) for low salt concentrations, shown as a straight dotted line, presents a factor of +1, indicating full dissociation of the ionic species in the PEO homopolymer. Indeed, the degree of dissociation for both PEO/LiTFSI and PEO/Li_2S_4 electrolytes at low R is close to unity. This implies that at low salt concentrations, both salts solubilize in PEO to release Li^+. However, remarkably for the same PEO homopolymer, there is about a factor of 4x reduction in the σ of Li_2S_4 compared to LiTFSI salt. This may indicate slower mobility of ions in general in PEO/Li_2S_4 complexes as compared to PEO/LiTFSI and/or a change in the transport number due to disulfide anion interactions with the PEO matrix. The lithium transference number (T^+) of PEO/Li_2S_4 complexes was investigated and the results compared to the T^+ of PEO/LiTFSI are displayed in **Figure 6b**. The T^+ of PEO/Li_2S_4 (average T^+ of 0.5) is also about a factor of 4x higher than the PEO/LiTFSI (average T^+ of 0.12) counterpart. In the PEO/LiTFSI electrolyte system, it has been shown by molecular dynamics (MD) simulations that the Li^+ have a strong association with the ether oxygen of the PEO chains while the $TFSI^-$ anion has less intimacy if any, and therefore moves more freely in the volume of the polymer [57]. Therefore, the increased T^+ of Li_2S_4 means that on average the S_4^{2-} anion is slowed down as compared to the Li^+. If this assertion is true, then the mobility of the free Li^+ cations in both systems should be similar. In **Figure 6c**, the contribution of the Li^+ cations (σ^+) to the overall conductivity of the PEO/Li_2S_4 and the PEO/LiTFSI electrolytes are compared. As expected, the σ^+ of PEO/Li_2S_4 and PEO/LiTFSI electrolytes are similar. This implies that the Li^+ cations in the respective electrolyte systems, have similar mobilities and the variation in σ is only due to the reduction in anion dynamics (S_4^{2-} *vs*. $TFSI^-$). The S_4^{2-} anions interact with the ether of the PEO which slows down their local dynamics compared to $TFSI^-$. This could also mean that the solvation of anions and cations can be more complex with the formation of clusters which further reduces their dynamics and mobility. In that case, the Li^+ cation could either interact partially with the PEO and the S_4^{2-} anion or the Li^+ can be linked to two anions. To investigate further the origin of the variation in σ, restricted diffusion measurement was used to calculate the ambipolar diffusion coefficient (D_{amb}) of the ionic species; Li_2S_4 and LiTFSI in the PEO and the results are displayed in **Figure 6d**. Within the investigated concentration range, the D_{amb} is constant and independent of R for both ionic species. However, the diffusion of Li_2S_4 in the PEO is reduced by several factors compared to the LiTFSI. To go further in investigating the contribution of each ionic species to the overall D_{amb}, **Eq. 14** and **15** were used to calculate the cationic (D^+) and anionic (D^-) diffusion coefficients respectively. The plot of D^+ with R in **Figure 6f**, shows that indeed the dissociated Li^+ in both Li_2S_4 and LiTFSI salts diffuse at the same speed and this speed is constant irrespective of the salt concentration. On the other hand, the plot of D^- *vs*. R in **Figure 6e**, expectedly displays close to an order of magnitude reduction in the diffusion of the S_4^{2-} anion in comparison to the $TFSI^-$. This is evidence that PEO homopolymer can reduce the shuttling of short-chain polysulfides

(S_4^{2-}) by two orders of magnitude (10^{-8} $cm^2.s^{-1}$) relative to conventional liquid electrolytes such as DOL/DME (10^{-6} $cm^2.s^{-1}$) used in Li-S battery [58].

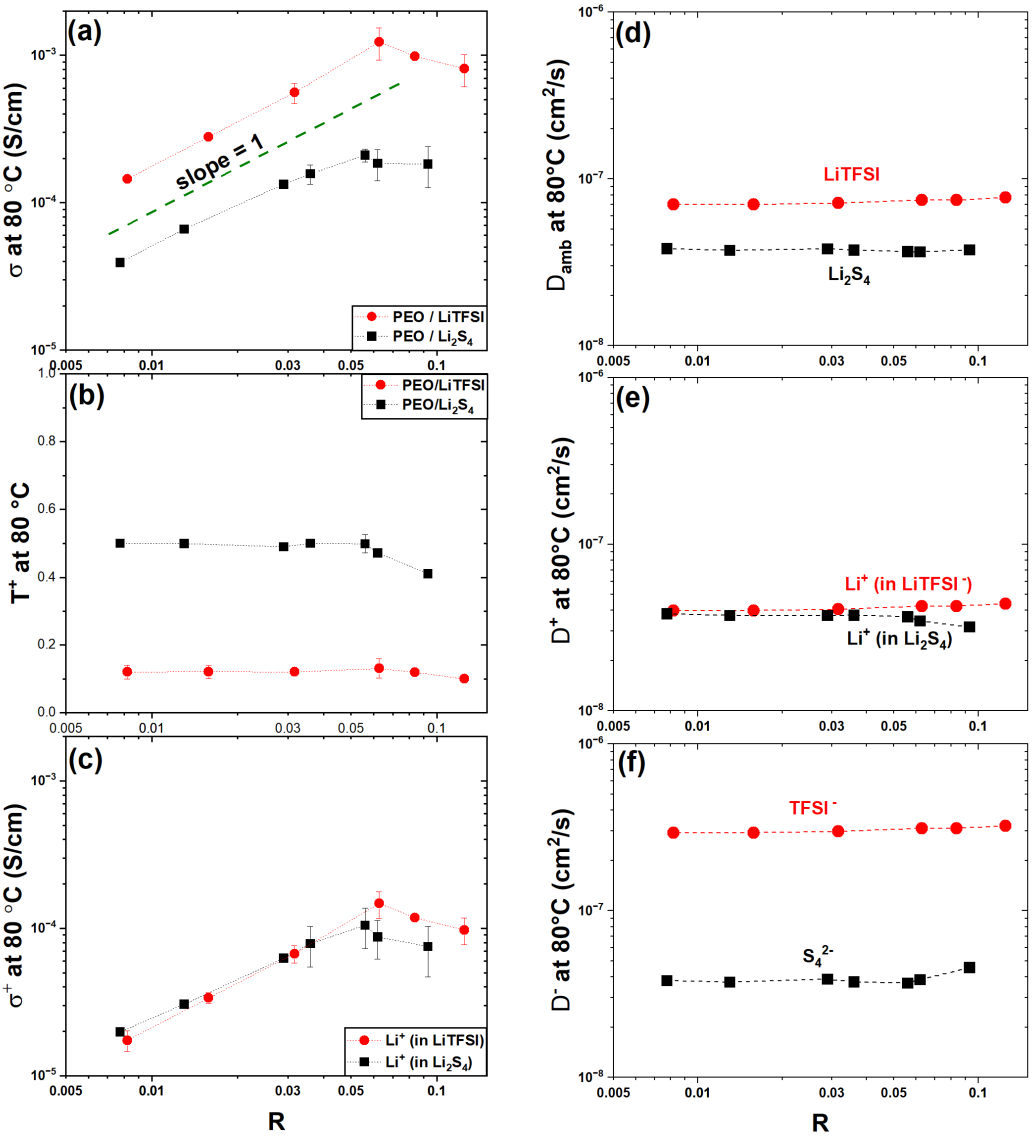

Figure 6. The plot of the (a) ionic conductivity (σ) at 80 °C, (b) Li^+ transference number (T^+) and (c) Li^+ conductivity (σ^+) of Li_2S_4. The straight dotted lines (green) in (a) represent the full dissociation (slope = 1) of Li^+ at low R. Also shown are the (d) ambipolar diffusion coefficient (D_{amb}), (e) Li^+ diffusion coefficient (D^+) and S_4^{2-} diffusion coefficient (D^-) in PEO.

2.6 Ionic transport of Li_2S_8 in PEO homopolymer

The ionic transport properties of Li_2S_8 in PEO homopolymer were also investigated to analyse the polymer's efficiency in mitigating the shuttling of the long-chain polysulfide. The plot of conductivity σ as a function of Li_2S_8 concentration (R) is shown in **Figure 7a**. Like PEO/LiTFSI, σ of the PEO/Li_2S_8 electrolyte increases with R until reaching a plateau at $R = 0.03$. But at $R \leq 0.03$, σ the PEO/Li_2S_8 is more than a factor of 2 lower than that of PEO/LiTFSI, nevertheless higher than that of PEO/Li_2S_4. This is in good agreement with the results of the T_g in **Figure 3a**. At $R > 0.03$, σ

of PEO/Li_2S_8 decreases sharply to more than an order of magnitude lower than that of PEO/LiTFSI. This could be a result of increased ion-ion cluster formation leading to high viscosity owing to the full dissociation of $2Li^+$ from the S_8^{2-} as in the equation $Li_2S_8 \rightarrow 2Li^+ + S_8^{2-}$. The contribution of the transference number of the ionic species to the overall conductivity was investigated by measuring the T^+ of the PEO/Li_2S_8 electrolyte and the result is shown in **Figure 7b**. In the PEO homopolymer, the Li^+ transference number from Li_2S_8 is more than 4x higher than that from LiTFSI and slightly higher than that of Li_2S_4. This means reduced mobility of S_4^{2-} as compared to S_8^{2-} anions.

A comparison of the σ of PEO/Li_2S_8 and PEO/Li_2S_4 shows a difference of about a factor of 2. This difference could originate from the transference number or the degree of dissociation of the two salts in PEO. Since the transference number of both salts in PEO is similar, the difference in dissociation of the salts in PEO may give rise to different σ. Indeed, from the T_m analysis, we see that Li_2S_8 is more soluble than Li_2S_4. We can therefore assume that the dissociation of Li_2S_4 in PEO will proceed by $Li_2S_4 \rightarrow Li^+ + LiS_4^-$. On the other hand, Li_2S_8 may fully solubilize in PEO to release $2Li^+$ cations according to the equation: $Li_2S_8 \rightarrow 2Li^+ + S_8^{2-}$. Overall, for LiS_4^- (in Li_2S_4), we can imagine a charge of -1 which is distributed over four sulfur atoms whereas for S_8^{2-} (in Li_2S_8), we would have a charge of -2 distributed over eight sulfur atoms. Therefore, the true equivalent concentration of Li^+ in Li_2S_8 will be $2R$. In **Figure 7c**, the plot of σ^+ versus R is shown, where the concentration of Li^+ cations in Li_2S_8 has been taken to be $2R$. At $R \leq 0.06$, the σ^+ of Li^+ in Li_2S_8 is similar to that of LiTFSI. This translates to similar Li^+ mobility in both systems. At higher R however, there is a deviation in the Li^+ for the two systems. To verify this, the D_{amb} of Li_2S_8 in PEO was measured using the restricted diffusion method and the results are presented in **Figure 7d**. The D_{amb} of Li_2S_8 is lower than that of LiTFSI as expected but it is also slightly lower than that of Li_2S_4. This means that despite the higher solubility of Li_2S_8 in PEO compared to Li_2S_4, its mobility is slightly reduced. The result of the calculation of the cationic diffusion coefficient (D^+) using **eq. 14** is shown in **Figure 7e**. The plot shows that the dissociated Li^+ from Li_2S_8 diffuse slightly slower when compared to those from LiTFSI. The evolution of D^- versus R displayed in **Figure 5e** shows that the diffusion of S_8^{2-} is slightly lower than S_4^{2-}. This could stem from both the slightly higher viscosity of the PEO/Li_2S_8 electrolyte due to higher solubility and the bulky nature of the anion (8 sulfur atoms) as compared to S_4^{2-} (4 sulfur atoms). Overall, the difference between σ of Li_2S_8 (factor 2 lower) and Li_2S_4 (factor 4 lower) as compared to LiTFSI in PEO, could stem from the difference in the degree of dissociation between the two lithium polysulfides. Thus, Li^+ for Li_2S_4 versus $2Li^+$ for Li_2S_8.

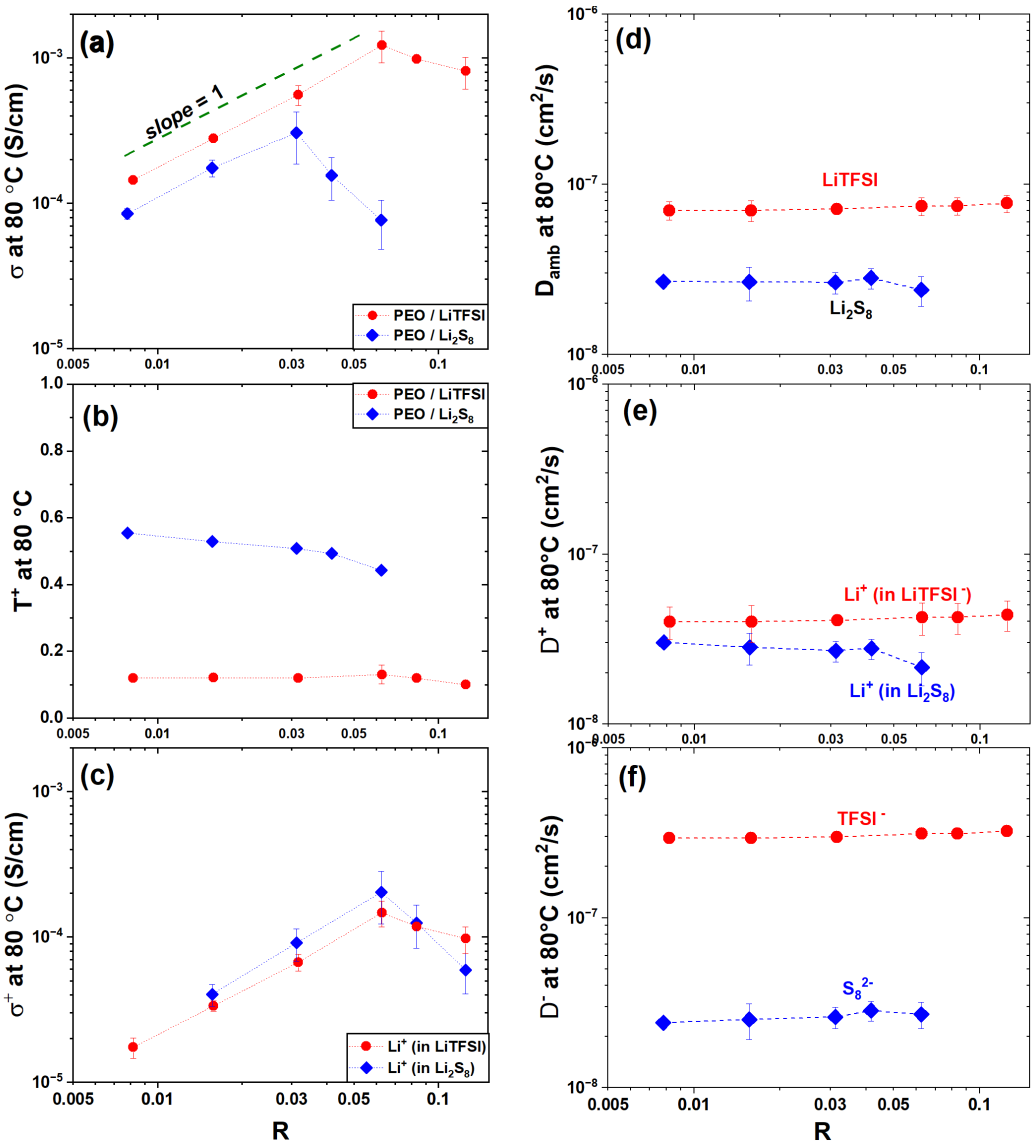

Figure 7. The plot of the (a) ionic conductivity (σ) at 80 °C, (b) Li^+ transport number (T^+) at 80 °C and (c) Li^+ conductivity (σ^+) of Li_2S_8. The straight dotted lines (green) in (a) represent the full dissociation (slope = 1) of Li^+ at low R. Also shown are the (d) ambipolar diffusion coefficient (D_{amb}) measured at 80 °C, (e) Li^+ diffusion coefficient (D^+) and S_8^{2-} diffusion coefficient (D^-) in PEO.

3 Conclusion

The thermodynamical properties of lithium polysulfides in PEO homopolymer were investigated via differential scanning calorimetry (DSC). The glass transition temperature (T_g) of the PEO/Li_2S_4 electrolytes showed a linear increase with salt concentration until a plateau at R = 0.04, indicative of the limit of solubility of Li_2S_4 into the PEO. On the contrary, the T_g of PEO/Li_2S_8 blends

increased continuously with *R*. This observation was further supported by the melting temperature (T_m), FTIR, density and XRD measurements of the PEO/Li_2S_x electrolytes revealing that the solubility of Li_2S_8 into PEO is higher than Li_2S_4. The electrochemical characterization of the PEO/Li_2S_x electrolytes indicates that Li_2S_4 may dissociate partially in PEO to form Li^+ and LiS_4^- species because of the limited solubility of the polysulfide into the homopolymer whereas the Li_2S_8 tends to fully dissociate. Furthermore, it was demonstrated that PEO can slow down the mobility of short-chain polysulfide (S_4^{2-}) anion by an order of magnitude relative to $TFSI^-$ anion while the Li^+ in both systems diffuse at the same speed. Due to the higher solvation of Li_2S_8 by PEO, the long-chain polysulfide can dissociate into $2Li^+$ cations and S_8^{2-} anion resulting in higher ionic conduction in the PEO/Li_2S_8 electrolyte compared to the PEO/Li_2S_4 system. The diffusion of S_8^{2-} (2×10^{-8} $cm^2.s^{-1}$) in PEO at 80 °C was found to be slightly slower than that of the S_4^{2-} (3×10^{-8} $cm^2.s^{-1}$). These results are intended to guide the design of SPEs used as binders or electrolyte layers to mitigate the transport of Li_2S_x in all solid-state Li-S batteries.

4 Declaration of Competing Interest

The authors declare that they have no known competing financial interests or personal relationships that could have appeared to influence the work reported in this paper.

5 Data availability

Data will be made available on request.

6 Acknowledgments

This work was supported by the French Agence Nationale de la Recherche ANR grant SHUTTLE (ANR19-CE05-0023).

7 References

1. Tarascon, J. M., and Armand, M., "Issues and challenges facing rechargeable lithium batteries," *Nature*, 414, 2001, 359–367.
2. Wang, Z., Liu, J., Wang, M., Shen, X., Qian, T., and Yan, C., "Toward safer solid-state lithium metal batteries: a review," *Nanoscale Adv.*, 2, 2020, 1828–1836.
3. Bruce, P. G., "Energy storage beyond the horizon: Rechargeable lithium batteries," *Solid State Ion.*, 179, 2008, 752–760.
4. Bruce, P. G., Freunberger, S. A., Hardwick, L. J., and Tarascon, J.-M., "Li-O_2 and Li-S batteries with high energy storage," *Nature Mater.*, 11, 2011, 19–29.
5. Bonnick, P., and Muldoon, J., "The Dr Jekyll and Mr Hyde of lithium sulfur batteries," *Energy Environ. Sci.*, 13, 2020, 4808-4833.
6. Allen J. Bard, Larry R. Faulkner, "Electrochemical methods: Fundamentals and applications," 2nd Edition, John Wiley & Sons, INC., New York, 2000.
7. Nitta, N., Wu, F., Lee, J. T., and Yushin, G., "Li-ion battery materials: present and future," *Mater. Today*, 18, 2015, 252–264.
8. Balsara, N. P., and Newman, J., "Comparing the energy content of batteries, fuels, and materials," *J. Chem. Educ.*, 90, 2013, 446–452.
9. Ji, X., and Nazar, L. F., "Advances in Li–S batteries," *J. Mater. Chem.*, 20, 2010, 9821-9826.
10. Li, G., Wang, S., Zhang, Y., Li, M., Chen, Z., and Lu, J., "Revisiting the role of polysulfides in lithium-sulfur batteries," *Adv. Mater.*, 30, 2018, 1705590.
11. Su, Y.-S., and Manthiram, A., "Lithium-sulphur batteries with a microporous carbon paper as a bifunctional interlayer," *Nat Commun.*, 3, 2012, 1166.
12. Wang, D.-W., Zhou, G., Li, F., Wu, K.-H., Lu, G. Q. M., Cheng, H.-M., and Gentle, I. R., "A microporous-mesoporous carbon with graphitic structure for a high-rate stable sulfur cathode in carbonate solvent-based Li-S batteries," *Phys. Chem. Chem. Phys.*, 14, 2012, 8703–8710.
13. Balach, J., Jaumann, T., Klose, M., Oswald, S., Eckert, J., and Giebeler, L., "Improved cycling stability of lithium–sulfur batteries using a polypropylene-supported nitrogen-doped mesoporous carbon hybrid separator as polysulfide adsorbent," *J. Power Sources*, 303, 2016, 317–324.
14. Chung, S.-H., Han, P., Singhal, R., Kalra, V., and Manthiram, A., "Electrochemically stable rechargeable lithium-sulfur batteries with a microporous carbon nanofiber filter for polysulfide," *Adv. Energy Mater.*, 5, 2015, 1500738.

15. Chung, S.-H., and Manthiram, A., “Bifunctional Separator with a light-weight carbon-coating for dynamically and statically stable lithium-sulfur batteries,” *Adv. Funct. Mater.*, 24, 2014, 5299–5306.

16. Huang, C., Xiao, J., Shao, Y., Zheng, J., Bennett, W. D., Lu, D., Saraf, L. V., Engelhard, M., Ji, L., Zhang, J., Li, X., Graff, G. L., and Liu, J., “Manipulating surface reactions in lithium-sulphur batteries using hybrid anode structures,” *Nat. Commun.*, 5, 2014, 3015.

17. Li, N.-W., Yin, Y.-X., Yang, C.-P., and Guo, Y.-G., “An artificial solid electrolyte interphase layer for stable lithium metal anodes,” *Adv. Mater.*, 28, 2016, 1853–1858.

18. Zhao, J., Zhou, G., Yan, K., Xie, J., Li, Y., Liao, L., Jin, Y., Liu, K., Hsu, P.-C., Wang, J., Cheng, H.-M., and Cui, Y., “Air-stable and freestanding lithium alloy/graphene foil as an alternative to lithium metal anodes,” *Nat. Nanotechnol.*, 12, 2017, 993–999.

19. Fang, R., Xu, H., Xu, B., Li, X., Li, Y., and Goodenough, J. B., “Reaction mechanism optimization of solid-state Li–S Batteries with a PEO-based electrolyte,” *Adv. Funct. Mater.*, 31, 2021, 2001812.

20. Hong, S., Wang, Y., Kim, N., and Lee, S. B., “Polymer-based electrolytes for all-solid-state lithium–sulfur batteries: from fundamental research to performance improvement,” *J. Mater Sci*, 56, 2021, 8358–8382.

21. Teran, A. A., and Balsara, N. P., “Effect of lithium polysulfides on the morphology of block copolymer electrolytes,” *Macromolecules*, 44, 2011, 9267–9275.

22. Wang, D. R., Wujcik, K. H., Teran, A. A., and Balsara, N. P., “Conductivity of block copolymer electrolytes containing lithium polysulfides,” *Macromolecules*, 48, 2015, 4863–4873.

23. Judez, X., Zhang, H., Li, C., González-Marcos, J. A., Zhou, Z., Armand, M., and Rodriguez-Martinez, L. M., “Lithium Bis(fluorosulfonyl)imide/Poly(ethylene oxide) polymer electrolyte for all solid-state Li-S cell,” *J. Phys. Chem. Lett.*, 8, 9, 2017, 1956–1960.

24. Judez, X., Zhang, H., Li, C., Eshetu, G. G., Zhang, Y., González-Marcos, J. A., Armand, M., and Rodriguez-Martinez, L. M., “Polymer-Rich Composite Electrolytes for All-Solid-State Li-S Cells,” *J. Phys. Chem. Lett.*, 8, 2017, 3473–3477.

25. Eshetu, G. G., Judez, X., Li, C., Bondarchuk, O., Rodriguez-Martinez, L. M., Zhang, H., and Armand, M., “Lithium azide as an electrolyte additive for all-solid-state lithium-sulfur batteries,” *Angew. Chem. Int. Ed.*, 56, 2017, 15368–15372.

26. Griffin, L. O., “Physical constants of linear homopolymers,” Springer Science & Business Media, 2012.

27. Loo, W. S., Mongcopa, K. I., Gribble, D. A., Faraone, A. A., and Balsara, N. P., "Investigating the effect of added salt on the chain dimensions of Poly(ethylene oxide) through small-angle neutron scattering," *Macromolecules*, 52, 2019, 8724–8732.

28. Adenusi, H., Chass, G. A., Passerini, S., Tian, K. V., and Chen, G., "Lithium batteries and the Solid Electrolyte Interphase (SEI)—Progress and outlook," *Adv. Energy Mater.*, 13, 2023, 2203307.

29. Barai, P., Mistry, A., and Mukherjee, P. P., "Poromechanical effect in the lithium–sulfur battery cathode," *Extreme Mech. Lett.*, 9, 2016, 359–370.

30. Zhang, H., Liu, C., Zheng, L., Xu, F., Feng, W., Li, H., Huang, X., Armand, M., Nie, J., and Zhou, Z., "Lithium bis(fluorosulfonyl)imide/poly(ethylene oxide) polymer electrolyte," *Electrochim. Acta*, 133, 2014, 529–538.

31. Bruce, P. G., and Vincent, C. A., "Steady state current flow in solid binary electrolyte cells," *J. electroanal. chem. interfacial electrochem.*, 225, 1987, 1–17.

32. Watanabe, M., "Estimation of Li^+ transport number in polymer electrolytes by the combination of complex impedance and potentiostatic polarization measurements," *Solid State Ion.*, 28-30, 1988, 911–917.

33. Newman, J., and Chapman, T. W., "Restricted diffusion in binary solutions," *AIChE J.*, 19, 1973, 343–348.

34. Mullin, S. A., Stone, G. M., Panday, A., and Balsara, N. P., "Salt diffusion coefficients in block copolymer electrolytes," *J. Electrochem. Soc.*, 158, 2011, A619.

35. Park, C., Ronneburg, A., Risse, S., Ballauff, M., Kanduč, M., and Dzubiella, J., "Structural and transport properties of Li/S Battery electrolytes: Role of the polysulfide species," *J. Phys. Chem. C*, 123, 2019, 10167–10177.

36. Barchasz, C., Molton, F., Duboc, C., Leprêtre, J.-C., Patoux, S., and Alloin, F., "Lithium/sulfur cell discharge mechanism: an original approach for intermediate species identification," *Anal. Chem.*, 84, 2012, 3973–3980.

37. Berthier, C., Gorecki, W., Minier, M., Armand, M. B., Chabagno, J. M., and Rigaud, P., "Microscopic investigation of ionic conductivity in alkali metal salts-poly(ethylene oxide) adducts," *Solid State Ion.*, 11, 1983, 91–95.

38. Przylusky, J., and Wieczorek, W., "DSC studies of solid polymeric electrolytes," *J. Therm. Anal.*, 38, 1992, 2229–2238.

39. West, E. D., "The Heat Capacity of Sulfur from 25 to 450°, the Heats and temperatures of transition and fusion[1,2]," *J. Am. Chem. Soc.*, 81, 1959, 29-37.

40. Lascaud, S., Perrier, M., Vallee, A., Besner, S., Prud'homme, J., and Armand, M., "Phase diagrams and conductivity behavior of Poly(ethylene oxide)-molten salt rubbery electrolytes," *Macromolecules*, 27, 1994, 7469–7477.

41. Stolwijk, N. A., Heddier, C., Reschke, M., Wiencierz, M., Bokeloh, J., and Wilde, G., "Salt-concentration dependence of the glass transition temperature in PEO–NaI and PEO–LiTFSI polymer electrolytes," *Macromolecules*, 46, 2013, 8580–8588.

42. Rey, I., Lassègues, J. C., Grondin, J., and Servant, L., "Infrared and Raman study of the PEO-LiTFSI polymer electrolyte," *Electrochim. Acta*, 43, 1998, 1505–1510.

43. R Rey, I., Johansson, P., Lindgren, J., Lassègues, J. C., Grondin, J., and Servant, L., "Spectroscopic and theoretical study of $(CF_3SO_2)_2N^-$ ($TFSI^-$) and $(CF_3SO_2)_2NH$ (HTFSI)," *J. Phys. Chem. A*, 102, 1998, 3249–3258.

44. Dissanayake, M. A. K. L., and Frech, R., "Infrared spectroscopic study of the phases and phase transitions in poly(ethylene oxide) and poly(ethylene oxide)-lithium trifluoromethanesulfonate complexes," *Macromolecules*, 28, 1995, 5312–5319.

45. Kim, K., Kuhn, L., Alabugin, I. V., and Hallinan, D. T., "Lithium salt dissociation in diblock copolymer electrolyte using fourier transform infrared spectroscopy," *Front. Energy Res.*, 8, 2020, 569442.

46. Liang, X., Hart, C., Pang, Q., Garsuch, A., Weiss, T., and Nazar, L. F., "A highly efficient polysulfide mediator for lithium-sulfur batteries," *Nat. Commun*, 6, 2015, 5682.

47. Evers, S., Yim, T., and Nazar, L. F., "Understanding the nature of absorption/adsorption in nanoporous polysulfide sorbents for the Li–S battery," *J. Phys. Chem. C*, 116, 37, 2012, 19653–19658.

48. Fang, R., Xu, B., Grundish, N. S., Xia, Y., Li, Y., Lu, C., Liu, Y., Wu, N., and Goodenough, J. B., "Li_2S_6-integrated PEO-based polymer electrolytes for all-solid-state lithium-metal batteries," *Angew. Chem.*, 133, 2021, 17842–17847.

49. Payne, D. R., and Wright, P. V., "Morphology and ionic conductivity of some lithium ion complexes with poly(ethylene oxide)," *Polymer*, 23, 982, 690–693.

50. Appetecchi, G. B., Henderson, W., Villano, P., Berrettoni, M., and Passerini, S., "PEO-$LiN(SO_2CF_2CF_3)_2$ polymer electrolytes: I. XRD, DSC, and ionic conductivity characterization," *J. Electrochem. Soc.*, 148, 2001, A1171-A1178.

51. Marzantowicz, M., Dygas, J. R., Krok, F., Nowiński, J. L., Tomaszewska, A., Florjańczyk, Z., and Zygadło-Monikowska, E., "Crystalline phases, morphology and conductivity of PEO:LiTFSI electrolytes in the eutectic region," *J. Power Sources*, 159, 2006, 420–430.

52. Fonseca, C., and Neves, S., “Characterization of polymer electrolytes based on poly(dimethyl siloxane-co-ethylene oxide),” *J. Power Sources*, 104, 2002, 85–89.

53. Rey, I., Bruneel, J.-L., Grondin, J., Servant, L., and Lassègues, J.-C., “Raman spectroelectrochemistry of a lithium/polymer electrolyte symmetric cell,” *J. Electrochem. Soc.,* 145, 1998, 3034–3042.

54. Bouchet, R., Lascaud, S., and Rosso, M., “An EIS study of the anode Li/PEO-LiTFSI of a Li polymer battery,” *J. Electrochem. Soc.*, 150, 10, 2003, A1385-A1389.

55. Hoffman, Z. J., Shah, D. B., and Balsara, N. P., “Temperature and concentration dependence of the ionic transport properties of poly(ethylene oxide) electrolytes,” *Solid State Ion.*, 370, 2021, 115751.

56. Villaluenga, I., Pesko, D. M., Timachova, K., Feng, Z., Newman, J., Srinivasan, V., and Balsara, N. P., “Negative Stefan-Maxwell diffusion coefficients and complete electrochemical transport characterization of homopolymer and block copolymer electrolytes,” *J. Electrochem. Soc.*, 165, 2018, A2766-A2773.

57. Borodin, O., and Smith, G. D., “Mechanism of ion transport in amorphous poly(ethylene oxide)/litfsi from molecular dynamics simulations,” *Macromolecules*, 39, 2006, 1620–1629.

58. Safari, M., Kwok, C. Y., and Nazar, L. F., “Transport properties of polysulfide species in lithium-sulfur battery electrolytes: coupling of experiment and theory,” *ACS Central Sci.*, 2, 2016, 560–568.